



OPEN

SUBJECT AREAS:

NANOPARTICLES
NANOPHOTONICS AND
PLASMONICSReceived
25 March 2014Accepted
9 May 2014Published
28 May 2014Correspondence and
requests for materials
should be addressed to
H.W.S. (songhw@jlu.
edu.cn)

Ag-SiO₂-Er₂O₃ Nanocomposites: Highly Effective Upconversion Luminescence at High Power Excitation and High Temperature

Wen Xu¹, Xiaolei Min¹, Xu Chen¹, Yongsheng Zhu², Pingwei Zhou¹, Shaobo Cui¹, Sai Xu¹, Li Tao¹ & Hongwei Song¹¹State Key Laboratory on Integrated Optoelectronics, College of Electronic Science and Engineering, Jilin University, 2699 Qianjin Street, Changchun 130012, China, ²College of Physics, Jilin University, 2699 Qianjin Street, Changchun 130012, China.

Rare Earth (RE) activated upconversion phosphors (UCPs), have demonstrated significant application potentials in some front fields, including solar energy conversion and bio-application. However, some bottleneck problems should be overcome, such as the lower upconversion efficiency, narrower excitation band, concentration-quenching and temperature-quenching. To solve these problems, the Ag-SiO₂-Er₂O₃ nanocomposites were fabricated, in which the upconversion luminescence (UCL) of Er₂O₃ was white broadband. Through the interaction of Er₂O₃ with surface plasmon (SP) of silver nanoparticles (SNPs), the threshold power for generating broadbands was suppressed largely in contrast to the Er₂O₃ nanoparticles (NPs), while the UCL brightness was enhanced remarkably, ranging from several to 10⁴ times, which strongly depended on the power density of excitation light. At excitation power density of 1.50 W/mm² of 980 nm light, the UCL intensity of Ag-SiO₂-Er₂O₃ is 40-folds than the well-known NaYF₄:Yb³⁺,Er³⁺ commercial powders. And more, it is also interesting to observe that the composites demonstrate two excitation bands extending of 780–980 nm, highly improved UCL with elevated temperature and excitation power density. The UCL mechanism related to UCL enhancement was carefully studied.

UCL, which can convert infrared (IR) radiation into visible light via a two-photon or multi-photon absorption process, has attracted extensive interests because of their potential applications in the field of upconversion lasers, IR quantum counters, three-dimensional (3D) displays, in vivo fluorescence imaging and et al^{1–5}. Among various UCP, some RE ions (such as Er³⁺/Yb³⁺ or Tm³⁺/Yb³⁺) co-doped fluoride phosphors are most favorable under 980-nm excitation, because of their sufficient absorption, matching energy levels and low phonon threshold, which lead to relatively efficient UCL⁶. Yet, these UCL have some disadvantages, which can not satisfy the requirement of various practical applications. First of all, their upconversion efficiency is still low, for instance, bulk NaYF₄:Yb³⁺, Er³⁺ in hexagonal phase, which is commonly considered as the most efficient UCP, its efficiency is only 3% under 980-nm excitation. And the strength of corresponding nanosized phosphor (<20 nm) is only one of tenth of the bulk^{7–8}. Second, because of the presence of the local thermal effect and saturation effect, the UCL intensity will saturate and even quench at relatively high excitation power density, which vitally influences the brightness of UCL⁹. Third, the temperature quenching phenomenon usually happens at high temperature, and the concentration quenching occurs as the concentration of activators is too high^{9,10}. In addition, for most of RE activated UCPs based on 4f-4f transitions, the excitation band is relatively narrow, which is difficult to satisfy the requirement of various optical devices, especially the requirement of solar spectrum conversion¹¹. Until now, it is still a challenge to obtain highly efficient UCPs, especially for applications under extreme conditions, such as high power excitation and high temperature.

Recently, Wang et al. observed that some lanthanide oxides micropowders, such as Yb₂O₃, Sm₂O₃, demonstrated efficient UC broadband emissions under the excitation of a 1 W 980-nm laser diode in vacuum, and the upconversion efficiency was estimated to be as high as 10%, and they attributed the broadband emissions to thermal avalanche¹². Further works were performed to identify the origin of the broadband emissions by Streck et al. and Wang et al^{13,14}. Streck attributed the broadband emissions to the charge transfer transition of Yb³⁺. Our group observed that some lanthanide oxides, such as Er₂O₃, Sm₂O₃, Nd₂O₃ and Pr₂O₃ demonstrated not only

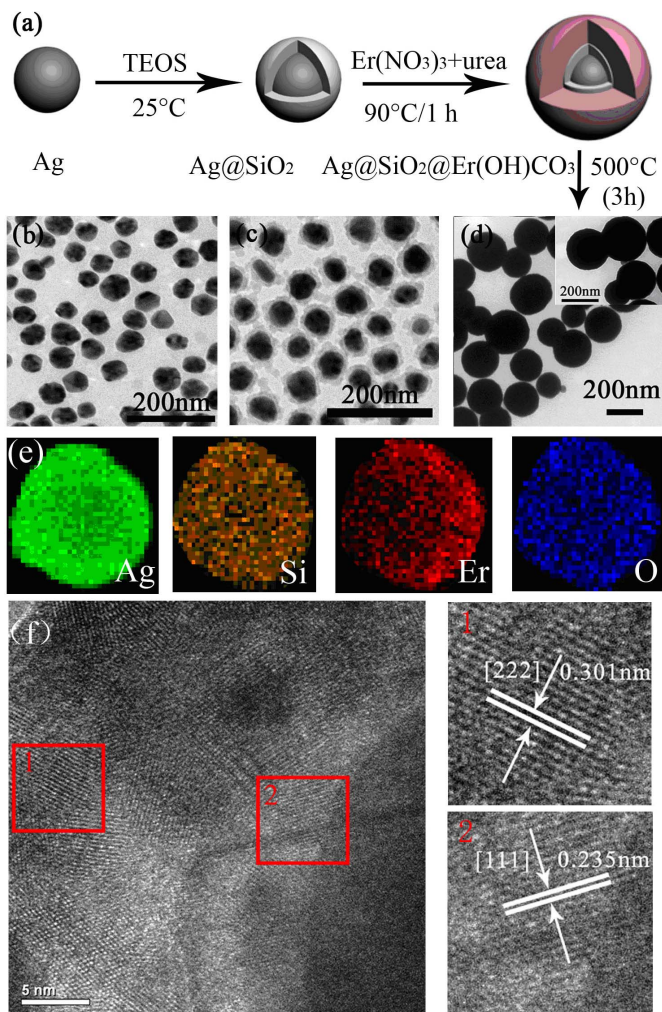


Figure 1 | (a) The specific preparing procedure of Ag-SiO₂-Er₂O₃ nanocomposites, (b-d) TEM images of the as as-prepared Ag NPs, Ag-SiO₂ composites, and Ag-SiO₂-Er₂O₃ nanocomposites, (e) the energy-dispersive X-ray (EDX) mapping of Ag-SiO₂-Er₂O₃ sample at the bottom of the figure, (f) the HR-TEM images of Ag-SiO₂-Er₂O₃ nanocomposites.

sufficient UC broadbands, but also sufficient IR broadbands, ranging of 1000–1700 nm under 980-nm excitation. The evolution of upconversion broadband of micro-sized Er₂O₃ with excitation power were studied, which showed that the broadbands actually came from the contribution of multi-transitions of Er³⁺ ions and spectral broadening of these transitions with elevated temperature¹⁵.

On the other hand, various methods have been explored to improve the strength/efficiency of UCL of nanophosphors^{16–19}. Surface enhanced fluorescence of emitters on rough noble metal surfaces is a promised way to largely enhance the UCL of RE doped nanophosphors^{20–22}. Recently, UCL enhancement based on the coupling of nanophosphors with noble metals such as gold and silver have been widely observed in UCPs, such as NaYF₄:Yb³⁺,Er³⁺ and NaYF₄:Yb³⁺,Tm³⁺. However, no literatures are related to the UCL enhancement of lanthanide oxides, a novel type of efficient UCP. In this paper, the Ag-SiO₂-Er₂O₃ nanocomposites were prepared to obtain effective enhancement of UCL. It is exciting to observe that in the composites, the UCL was improved an order of 10⁰–10⁴, depending of the excitation power density. And the UCL of Ag-SiO₂-Er₂O₃ composites was more effective than bulk NaYF₄:Yb,Er at the high power excitation and the high temperature environment. Furthermore, the UC broadband emission and UCL enhancement mechanism of Ag-SiO₂-Er₂O₃ nanocomposites were proposed.

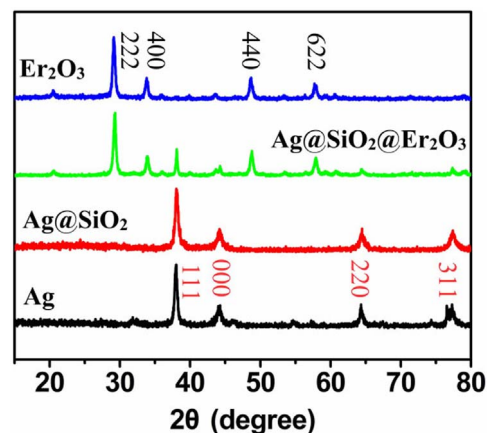


Figure 2 | XRD patterns of the Ag NPs, Ag-SiO₂ composites, Ag-SiO₂-Er₂O₃ composites samples.

Results and Discussion

Morphology and Structure. First, the morphology of Ag NPs, Ag-SiO₂, Ag-SiO₂-Er₂O₃ nanocomposites and Er₂O₃ NPs were examined by HR-TEM images, as shown in Fig. 1 (b–d). Fig. 1(b) shows the TEM image of the Ag NPs, which indicates that the Ag NPs are basically uniform and monodisperse, with an average diameter of ~60 nm. From Fig. 1(c), it can be distinguished that after coating with SiO₂, Ag-SiO₂ composites with core-shell structure are formed and the composites are monodisperse. The thickness of the SiO₂ shell is about 10–15 nm. In Fig. 1(d), it can be seen that after further coating with Er₂O₃, the sizes of Ag-SiO₂-Er₂O₃ composites grow to 150–200 nm and are sphere-like in shape. Because of large contrast of Er₂O₃, the internal structure of Ag-SiO₂-Er₂O₃ is unable to identify. The illustration of Fig. 1(d) shows the TEM image of Er₂O₃ NPs prepared by the same method, which shows that the diameter of Er₂O₃ NPs is about 150–200 nm, similar to Ag-SiO₂-Er₂O₃ NPs.

In order to further identify the internal structure of the Ag-SiO₂-Er₂O₃ nanocomposites, Fig. 1 (e) shows the EDX mapping to analysis of elements of Ag-SiO₂-Er₂O₃ sample. From left to right, they represent silver, silicon, erbium, and oxygen elements, respectively. It can be seen that all of the elements distribute homogeneously in the whole sphere. Layer gradient distribution of elements can not be identified. This suggests that all the elements have been diffused after annealing at 500°C. In the fringe patterns of the Ag-SiO₂-Er₂O₃ nanocomposites (Fig. 1 (f)), two different fringe spacing was determined to be ~0.301 nm and ~0.231 nm, which corresponded closely with the spacing of the (222) plane of cubic Er₂O₃ (0.307 nm) (JCPDS No. 77-0464) and the (111) plane of fcc silver (0.235 nm) (JCPDS No. 87-0717), respectively. From the HR-TEM, we can further deduce the forming of Ag-SiO₂-Er₂O₃ nanocomposites.

Fig. 2 shows the XRD patterns of the samples Ag NPs, Ag-SiO₂ composites, Ag-SiO₂-Er₂O₃ nanocomposites. Comparing to the corresponding standard cards, it can be seen that silver and Er₂O₃ NPs in pure cubic phase are formed. And, after coating with SiO₂ shells, no extra patterns could be identified except Ag NPs, because SiO₂ shells are amorphous in phase. In the Ag-SiO₂-Er₂O₃ composites, both XRD patterns of cubic silver and cubic Er₂O₃ could be identified, as shown in the figure, implying the formation of Ag-SiO₂-Er₂O₃ composites.

Fig. 3 shows the UV-Vis-Infrared absorption spectra of Ag NPs, Ag-SiO₂ composites and Ag-SiO₂-Er₂O₃ composites. It can be seen that the silver NPs demonstrate relatively narrow surface plasmon absorption (SPA), peaking around 420 nm. After coating with SiO₂ shell, the SPA of silver shifts toward red side due to the dielectric effect^{23,25}. It's interesting to observe that the SPA of Ag-SiO₂-Er₂O₃ composites demonstrates broadbands, extending from 350–1100 nm.

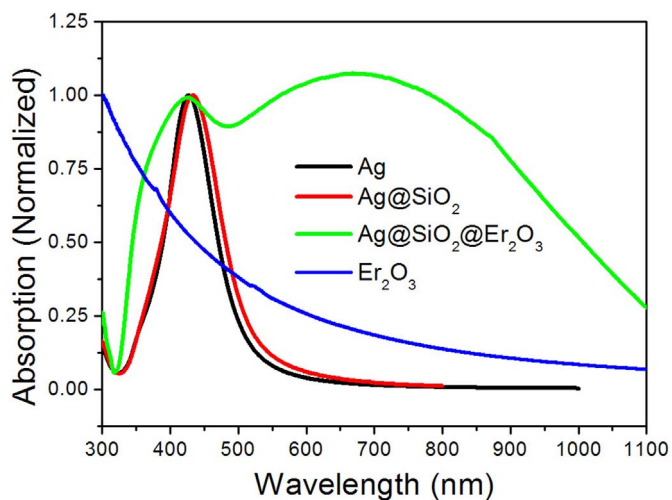


Figure 3 | The absorption spectra of Ag NPs, Ag-SiO₂ composites and the Ag-SiO₂-Er₂O₃ composites.

Two bands can be identified, one locates around 450 nm, and the other locates around 700 nm, corresponding to the transverse and longitude SPA of silver, respectively. Furthermore, as a comparison, the absorption spectrum of Er₂O₃ NPs was given in Fig. 3, it can be seen that there is no obvious peak, and with the decrease of wavelength the absorption increases, attributed to the scattering of the Er₂O₃ NPs. This suggests that, in the Ag-SiO₂-Er₂O₃ composites,

the silver NPs might have been changed into small NPs and these small NPs demonstrate anisotropic, leading to the occurrence of longitude SPA of silver.

UCL Enhancement of Ag-SiO₂-Er₂O₃ Nanocomposites. Fig. 4 (a) and Fig. 4 (b) show the UCL spectra of Er₂O₃ NPs and Ag-SiO₂-Er₂O₃ composites under the excitation of 0.26–1.41 W/mm² 980 nm light, respectively. It can be seen that, with relatively low excitation power, the emission spectra of Er₂O₃ and Ag-SiO₂-Er₂O₃ both have two groups of emission lines. The lines in the green range correspond to the ²H_{11/2}/⁴S_{3/2}-⁴I_{9/2} transitions, while those in the red range to the ⁴F_{9/2}-⁴I_{15/2} transitions, and the red emissions of ⁴F_{9/2}-⁴I_{15/2} are dominant for Er₂O₃ NPs. This is in consistent with the result of micro-sized Er₂O₃ and can be mainly attributed to the contribution of cross relaxation channels for Er³⁺ ions¹⁵. And with increasing the excitation power, a broadband emission ranging of 400–800 nm appears and the intensity ratio of the red to the green emission also decreases with the increasing excitation power. In addition, under the excitation of relatively high excitation power, both Er₂O₃ and Ag-SiO₂-Er₂O₃ NPs demonstrate broadband emissions, and their central positions both locate around 600 nm (~2 eV), independent of excitation power density. It should be highlighted that in contrast to Er₂O₃, the threshold power of generating white broadbands in the Ag-SiO₂-Er₂O₃ nanocomposites degraded from 0.65 W/mm² to 0.26 W/mm². In our previous work, the UCL of Er₂O₃ microsized powders was studied, which demonstrated considerable difference comparing to the present Er₂O₃ NPs and Ag-SiO₂-Er₂O₃ composites. As a comparison, the UCL spectra of bulk Er₂O₃ were shown in Fig. 4(c)¹⁵. In the bulk

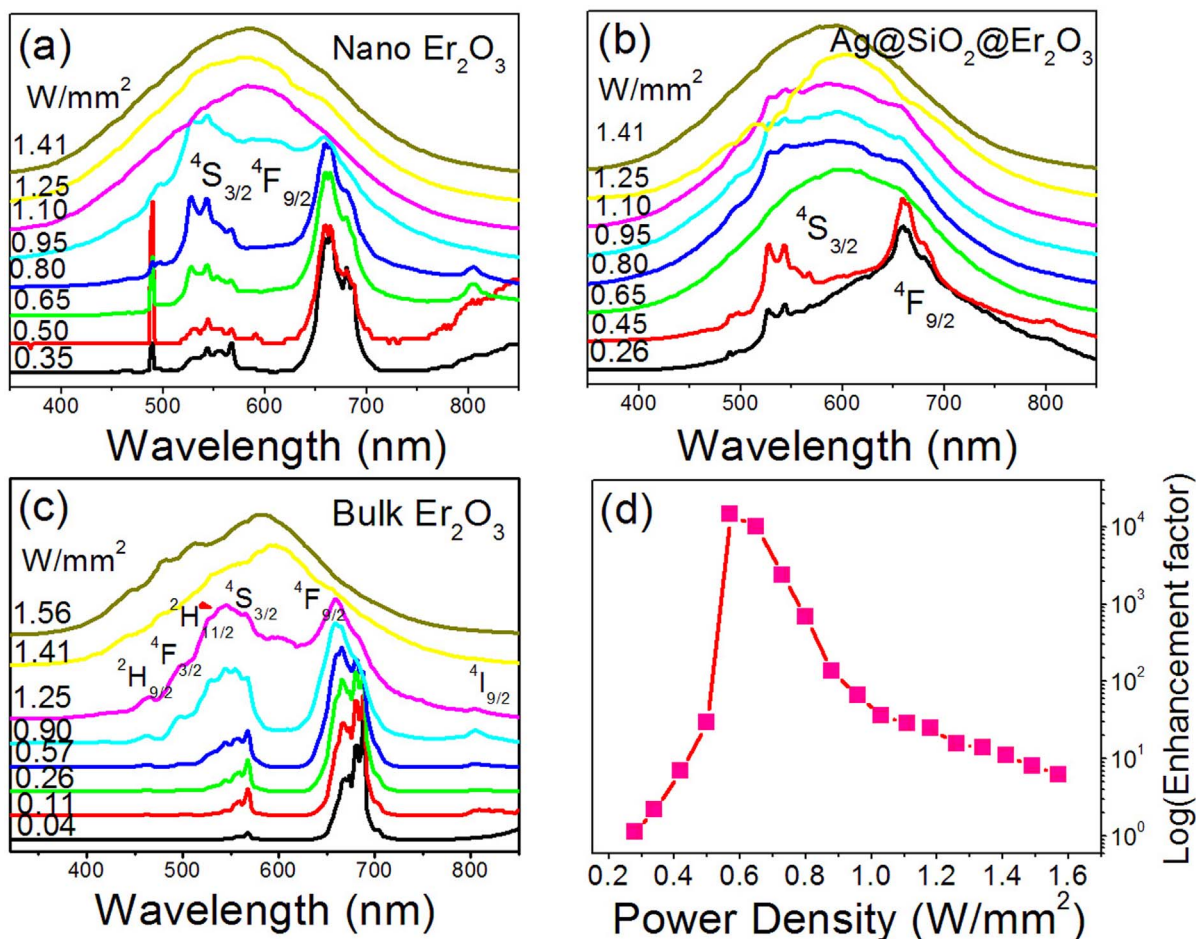


Figure 4 | (a–c) The UCL spectra of Er₂O₃ NPs, Ag-SiO₂-Er₂O₃ composites, and the UCL spectra of bulk Er₂O₃ under as a function of 980 nm excitation power density, respectively, (d) the UCL EF as a function of excitation power density.

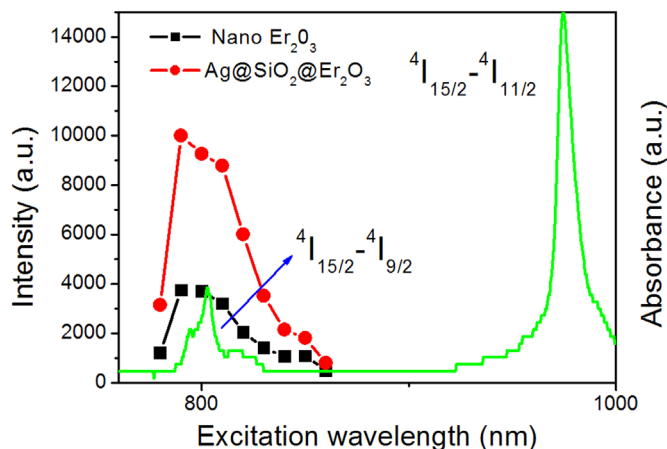


Figure 5 | The UC excitation spectra in a range 780–860 nm in Er_2O_3 NPs and $\text{Ag-SiO}_2\text{-Er}_2\text{O}_3$ nanocomposites, and the absorption spectra of Er^{3+} ions.

Er_2O_3 , the UCL of Er^{3+} ions originates from the emissions of Er^{3+} all the time. The generation of broadbands originates from the contribution of different transitions of Er^{3+} ions, ${}^2\text{H}_{9/2}/{}^4\text{F}_{3/2}\text{-}{}^4\text{I}_{15/2}$ (three-photons), ${}^2\text{H}_{11/2}/{}^4\text{S}_{3/2}\text{-}{}^4\text{I}_{15/2}$ (two-photon) and ${}^4\text{F}_{9/2}\text{-}{}^4\text{I}_{15/2}$ (three-photon) and their spectral broadening. In the Er_2O_3 NPs and $\text{Ag-SiO}_2\text{-Er}_2\text{O}_3$ composites, the broadband locates around 600 nm and is independent of excitation power, which is very similar to our previous result observed in $\text{YVO}_4:\text{Yb}^{3+}, \text{Er}^{3+}$ NPs²⁶. It could be attributed to the UCL of oxygen defects. Actually, the broadband UC emissions in lanthanide oxides are quite complex and their origins have not been clarified, and basically, they could be attributed to charge transfer transitions of rare earths, defect transitions, or electron-hole pairs^{13,27,28}. The mechanism will be discussed later in details.

Fig. 4(d) shows the UCL enhancement factor (EF, which is defined as the ratio of UCL intensity of the $\text{Ag-SiO}_2\text{-Er}_2\text{O}_3$ composites to that of Er_2O_3 NPs) as a function of excitation power density. It is interesting to see that the enhancement factor (EF) varies significantly with excitation power density, from several times to 10^4 times. At relative low excitation power, the UCL intensity of $\text{Ag-SiO}_2\text{-Er}_2\text{O}_3$ increases from several times to several ten times over that of Er_2O_3 . As the excitation power increases to 0.57 W/mm^2 , due to the sudden change of UCL (see Fig. 6), the enhancement factor dramatically increases to 9850 times, which shows that the UCL intensity of $\text{Ag-SiO}_2\text{-Er}_2\text{O}_3$ is about four orders higher than that of Er_2O_3 . As the excitation power density increases further, EF gradually decreases. And at relatively high excitation power density ($0.8\text{--}1.6 \text{ W/mm}^2$), EF gradually decreases to 7 times.

It is interesting to observe that, in the Er_2O_3 NPs, the UCL of the broadband was obtained not only under the excitation of 980 nm, corresponding to the excitation of ${}^4\text{I}_{15/2}\text{-}{}^4\text{I}_{11/2}$ transition of Er^{3+} ions, but also under the excitation of 780–860 nm laser, corresponding to the excitation of ${}^4\text{I}_{15/2}\text{-}{}^4\text{I}_{9/2}$ transition of Er^{3+} ions, as shown in Fig. 5. The UCL spectra of $\text{Ag-SiO}_2\text{-Er}_2\text{O}_3$ under the excitation of 808 nm light were recorded in Fig. S1, which showed that the UC emission bands extended of 400–750 nm, and the central emissions located at around 660 nm, corresponding to the ${}^4\text{F}_{9/2}\text{-}{}^4\text{I}_{15/2}$ transitions of Er^{3+} ions and the other transitions of Er^{3+} ions, ${}^2\text{H}_{11/2}/{}^4\text{S}_{3/2}\text{-}{}^4\text{I}_{15/2}$ and ${}^2\text{H}_{9/2}/{}^4\text{F}_{3/2}/{}^4\text{F}_{7/2}\text{-}{}^4\text{I}_{15/2}$ could also be identified. From the absorption spectra of Er^{3+} ions in Fig. 5, it's known that the absorption value of 808 nm is significantly lower than 980 nm, the achievement of UC broad band emission under 808 nm excitation should have higher excitation power density than that under 980 nm excitation. And the excitation power density of 808 excitation ($0.29\text{--}0.37 \text{ W/mm}^2$) in Fig S1 is lower than that with the 980 nm excitation, leading to the

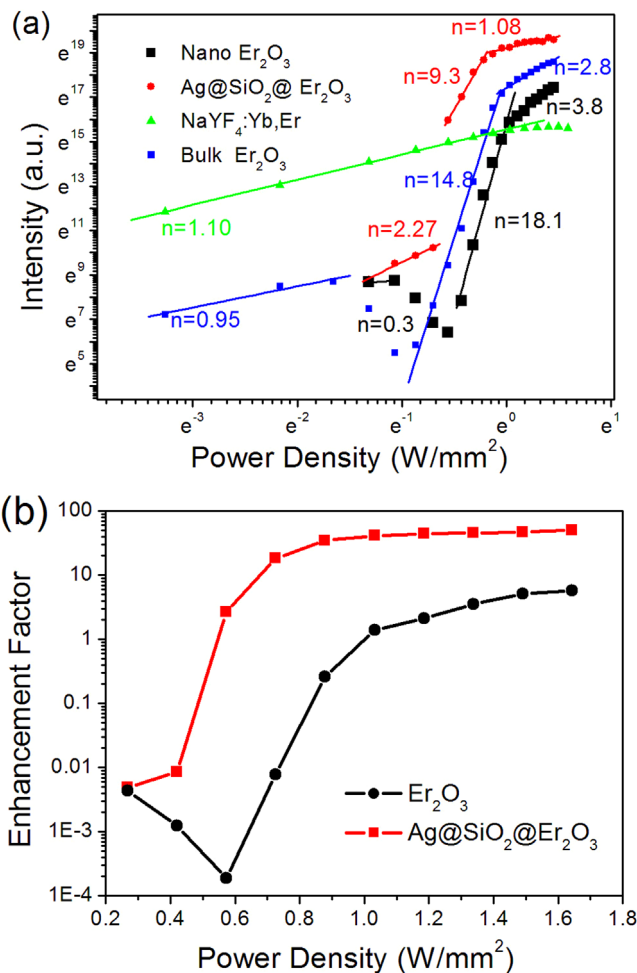


Figure 6 | (a) The power density dependence of integral UCL intensity of Er_2O_3 NPs, $\text{Ag-SiO}_2\text{-Er}_2\text{O}_3$ composites, bulk $\text{NaYF}_4:\text{Yb}, \text{Er}$, and bulk Er_2O_3 under 980 nm excitation; (b) the UCL EF as a function of excitation power density.

weaker UC broad band emission. Because the intrinsic transition of Er^{3+} (${}^4\text{F}_{9/2}\text{-}{}^4\text{I}_{15/2}$) is the main emission, leads to red-shift of the central emissions to 660 nm, so the broad band for 808 nm excitation is different from that for 980 nm excitation. In fact, we measured the UC broad band emission under 808 nm excitation (with excitation power density $\sim 6 \text{ W/mm}^2$, at the excitation spectra measurement), the broad band emission is exactly in accordance with those under 980 nm excitation. Furthermore, the UC excitation spectra in the range of 780–860 nm in Er_2O_3 NPs and $\text{Ag-SiO}_2\text{-Er}_2\text{O}_3$ nanocomposites were measured and compared (the excitation power density is $\sim 6 \text{ W/mm}^2$), as shown in Fig. 5. It should be noted that the UC broadband emission spectra are exactly in accordance with those under 980 nm excitation. With the excitation range of 780–860 nm, the obvious excitation bands were identified, centering around 790 nm, for both Er_2O_3 NPs and $\text{Ag-SiO}_2\text{-Er}_2\text{O}_3$ nanocomposites, which were in accordance with the ${}^4\text{I}_{15/2}\text{-}{}^4\text{I}_{9/2}$ excitation transition of Er^{3+} ions. In $\text{Ag-SiO}_2\text{-Er}_2\text{O}_3$ nanocomposites, the UCL enhancement of several times was observed in the whole range from 780 nm to 860 nm. The UCL enhancement in $\text{Ag-SiO}_2\text{-Er}_2\text{O}_3$ nanocomposites could be due to three reasons: First, under 780–980 nm excitation, corresponding to the longitude SPA of Ag NPs, ET from Ag NPs to Er_2O_3 happened effectively, leading to UCL enhancement of $\text{Ag-SiO}_2\text{-Er}_2\text{O}_3$ nanocomposites; Second, the excitation and emission strength enhanced due to the field enhancement effect; Third, the thermal effect happened with the surface plasmon excitation of Ag NPs, leading to the thermal avalanche



happening easily, and to the decrease of excitation threshold of the broadband emission.

In order to further confirm the mechanism of UCL enhancement, the Ag-SiO₂-Y₂O₃:10%Yb,1%Er nanocomposites as well as Y₂O₃:10%Yb, 1%Er were also investigated for comparison and the intrinsic transitions coming from Er³⁺ and the broadband were identified. The intrinsic transition of Er³⁺ ions was much higher than that of Er₂O₃ because of concentration quenching¹⁰ and broadband emission was significantly lower than that of Er₂O₃. In comparison to Y₂O₃:Yb³⁺,Er³⁺, the emission of Er³⁺ in Ag-SiO₂-Y₂O₃:Yb, Er was suppressed, while the broadband emission was improved. This suggests that the UCL enhancement of the broadband emission mainly originates from the thermal effect, instead of ET from Ag to Er₂O₃ or field enhancement effect (see Fig. S2).

Ag-SiO₂-Er₂O₃ Composites: Strong UCL at High Power Excitation and at High Temperature.

Fig. 6 (a) shows the power density dependence of integral UCL intensity of Er₂O₃ NPs and Ag-SiO₂-Er₂O₃ nanocomposites on excitation power density of 980 nm light in logarithmic coordinate. It can be seen that basically the power density dependence can be divided into three periods. For Er₂O₃ NPs, the overall UCL intensity first decreases slowly with the increasing excitation power before the generation of UC broadband. As the UC broadband appears, the UCL intensity increases dramatically with the increasing excitation power, with a power law of $I \sim P^n$ and the slope n is as high as 18.1. Then, as the excitation power continuously increases, the slope n drops to 3.8. For the Ag-SiO₂-Er₂O₃ composites, the UCL intensity increases with a slope of $n = 2.27$ before generation of the broadband. Then, a sudden increase occurs, accompanying the generation of UC broadband, and after that, the UCL intensity increases with a slope of $n = 9.3$. Finally, the slope drops to $n = 1.07$. Presently, the super-strong and complex power dependence of the UCL intensity has not been completely understood. It is suggested that during the UC process, photon avalanche or thermal avalanche probably happens¹². For comparison, the excitation power density dependence of integral UCL intensity (including ²H_{11/2}, ⁴S_{3/2}, ⁴F_{9/2}-⁴I_{15/2} transitions) of the bulk NaYF₄:Yb,Er were given in Fig. 6. The value of slope n was about 1.1, which was much smaller than the required photon number ($n = 2, 3$) populating to the corresponding levels. This can be attributed to the saturation effect as well as the local thermal effect induced by the laser exposure. And with further increasing the excitation power, the UCL intensity has a decrease in NaYF₄:Yb,Er. Fig. 6(b) shows the UCL enhancement factor (EF1, which is defined as the ratio of UCL intensity of Er₂O₃ and Ag-SiO₂-Er₂O₃ NPs to that of the NaYF₄:Yb,Er powders, respectively) as a function of excitation power density. From Fig. 6(b), it's observed that at lower excitation power density, the traditional UCL material such as NaYF₄:Yb,Er has great advantage because of the lower excitation threshold, however under higher power excitation, Er₂O₃ and Ag-SiO₂-Er₂O₃ nanocomposites has higher UCL intensity, because of the high saturation effect and the local thermal effect in NaYF₄:Yb³⁺, Er³⁺. It's worth noting that as the excitation power approached to 1.5 W/mm², the UCL strength of Ag-SiO₂-Er₂O₃ nanocomposites was 45 times over NaYF₄:Yb³⁺, Er³⁺ powders.

As is known, the concentration quenching phenomenon would happen especially in UCL material as the concentration of activators is too high because of cross relaxation, which limits the UCL strength of the RE activated UCP¹⁰. Recently, Jin et al. reported that high excitation irradiance could alleviate concentration quenching in UCL when combined with high activator concentration²⁹. In Er₂O₃ and Ag-SiO₂-Er₂O₃ NPs, which the concentration of activator was 100% in molar ratio, the similar phenomenon was also observed. As the excitation power density was lower, the concentration quenching happened seriously, which was confirmed by the much lower UCL intensity of Er₂O₃ in comparison to that of Y₂O₃:Yb,Er. However, at

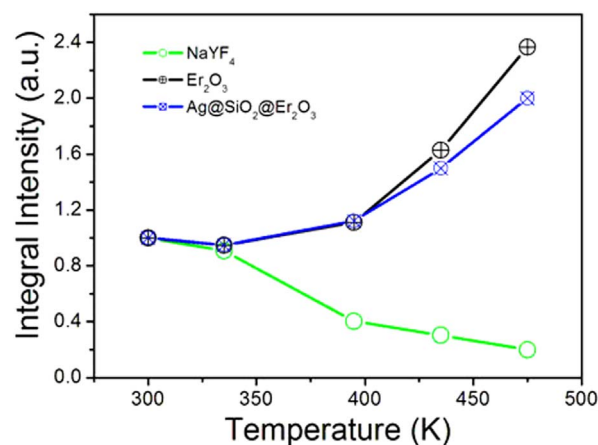


Figure 7 | The temperature dependence of the UCL integral intensity (normalized at 300 K) of Er₂O₃ NPs, Ag-SiO₂-Er₂O₃ composites, and bulk NaYF₄:Yb, Er on 980 nm light excitation.

sufficient excitation power, the effective UCL was generated for both nanosized and bulk Er₂O₃ (See Fig. 6), and Ag-SiO₂-Er₂O₃, implying the concentration quenching was perfectly suppressed (In the bulk Er₂O₃, the luminescent centers were contributed by Er³⁺ ions all the time, and in the nanosized samples, the generation of broadband originated from the excitation of Er³⁺ ions).

Furthermore, the temperature dependence of the UCL integral intensity (normalized at 300 K) under 1.10 W/mm² 980 nm excitation were recorded for nanosized Er₂O₃, Ag-SiO₂-Er₂O₃, and bulk NaYF₄:Yb, Er in the range of 300–475 K, as shown in Fig. 7. It's exciting to observe that the integral intensity increases 2.4 fold and 2.0 fold for Er₂O₃ and Ag-SiO₂-Er₂O₃, respectively, while reduces to the 20% of original for NaYF₄:Yb,Er as the temperature increases from 300 K to 475 K, implying significant temperature quenching. For Er₂O₃ and Ag-SiO₂-Er₂O₃ composite, the high temperature promotes the photon avalanche, leading to the increase of the UC broad emission with the increasing temperature. From the results, we can deduce that it's difficult to realize effective UCL in traditional materials (such as NaYF₄:Yb,Er,) at high power excitation, high concentration activator and high temperature conditions. While for Ag-SiO₂-Er₂O₃ composite, it overcomes these problems, which has great significance in extreme conditions.

The origin of UC Broadband Emission. In order to better understand the origin of the UCL process, the temperature and photocurrent, as a function of excitation power density in the Er₂O₃ NPs and Ag-SiO₂-Er₂O₃ nanocomposites samples under 980 nm excitation, were recorded in Fig. 8. The temperature measurement under the exposure of 980 nm light was achieved by burying the thermocouple thermometer into the powder plate samples. In Fig. 8(a), it can be seen that, in Er₂O₃ NPs and Ag-SiO₂-Er₂O₃ nanocomposites, the temperature varies from 375 K to 600 K, 470 K to 680 K under the excitation power ranging from 0.25 W/mm² to 1.5 W/mm², respectively. And Ag-SiO₂-Er₂O₃ nanocomposites have higher temperature than that of Er₂O₃. And the temperature of broadband emission happening is about 460 K for the two samples. The irradiation power density corresponding to 460 K for the Ag-SiO₂-Er₂O₃ nanocomposites is lower than that for the Er₂O₃ sample (the necessary temperature for generating holes in the valence band). This indicates that the occurrence of broadband UCL is accompanied by the generation of thermal holes in valence band. And such the high temperature generates thermal holes in the valence band. It should be noted that the temperature is much lower than the necessary temperature for generating sufficient blackbody radiation (~2500 K)³⁰. The power density dependence of the photocurrent of Er₂O₃ NPs and Ag-SiO₂-Er₂O₃ nanocomposites

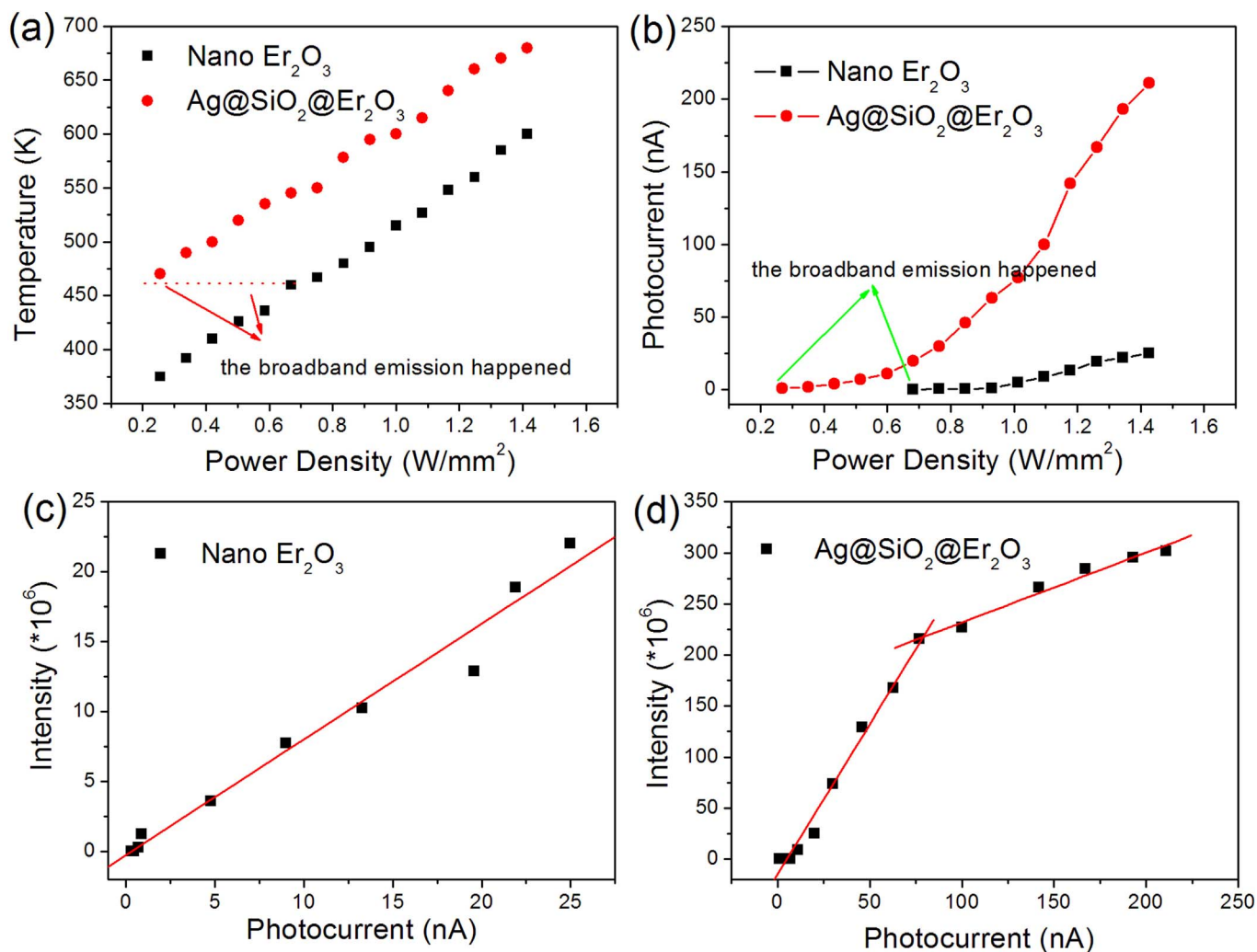


Figure 8 | The temperature (a) and photocurrent (b) as a function of excitation power density in the Er_2O_3 and $\text{Ag-SiO}_2\text{-Er}_2\text{O}_3$ nanocomposites samples under 980 nm excitation, the UCL intensity of Er_2O_3 (c) and $\text{Ag-SiO}_2\text{-Er}_2\text{O}_3$ composites (d) as a function of the photocurrent.

was shown in Fig. 8b. The photocurrent increases with the excitation power density, which is along with generating the UC broadband. And the photocurrent has higher value in $\text{Ag-SiO}_2\text{-Er}_2\text{O}_3$ nanocomposites. It's interesting to observe that the integral intensity of UC broadband in Er_2O_3 and $\text{Ag-SiO}_2\text{-Er}_2\text{O}_3$ nanocomposites satisfies with the linear dependencies with the photocurrent increasing (Fig. 8c–d). From Fig. S3, the photocurrent increases dramatically with the increasing excitation power, with a power law of $I_c \sim P^n$ and the slope n is 6.9 and 3.8 in Er_2O_3 and $\text{Ag-SiO}_2\text{-Er}_2\text{O}_3$ nanocomposites, respectively. The high slope n of UC broadband ($I \sim P^n$) would be attributed to the high slope n of photocurrent ($I_c \sim P^n$). Furthermore, the temperature dependent photocurrent of Er_2O_3 and $\text{Ag-SiO}_2\text{-Er}_2\text{O}_3$ composites was shown in Fig. 9. According to the Boltzmann distribution, the relationship between the electrical conductivity σ and the temperature T can be written as, $\sigma = \sigma_0 e^{-\frac{\Delta E}{k_0 T}}$, where k_0 is Boltzmann's constant, ΔE is the energy difference between the valence band maximum of Er_2O_3 and the unknown confined state in the bandgap (Most of RE_2O_3 compounds were p-type semiconductors.[31]). According to Figure Fig. 9, ΔE was deduced to be 1.11 eV and 1.21 eV. As to the origin of the unknown state, has not been clarified. Here, we suggest that the excited state of Er^{3+} ($^4I_{13/2}$) is the possible candidate of the confined state (its ground state locates above the valence band maximum).

Recently, Strek et al. have also observed UC broadband in $\text{LiYbP}_4\text{O}_{12}$ and its origin was attributed to the radiative charge transfer transitions of Yb^{3+} or Yb^{2+} ¹³. According to the literatures, the

charge transfer (CT) emissions of Yb^{2+} and Yb^{3+} located at around 560 nm (~ 2.2 eV) and 650 nm (~ 1.9 eV) in oxide compounds, respectively, which was different from the present result at 600 nm (~ 2.0 eV). In our previous work, in $\text{YVO}_4:\text{Yb}$, Ln^{3+} (Er^{3+} , Tm^{3+} ,

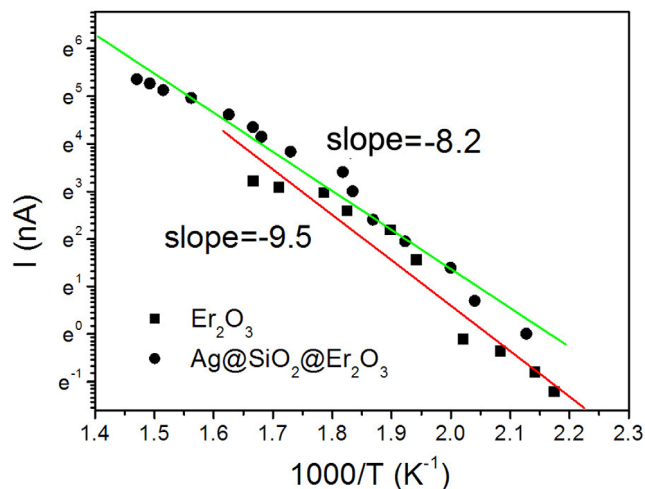


Figure 9 | The plot of natural logarithm of the photocurrent (I) against the reciprocal of absolute temperature in Er_2O_3 and $\text{Ag-SiO}_2\text{-Er}_2\text{O}_3$ composites under the excitation of 980 nm light.

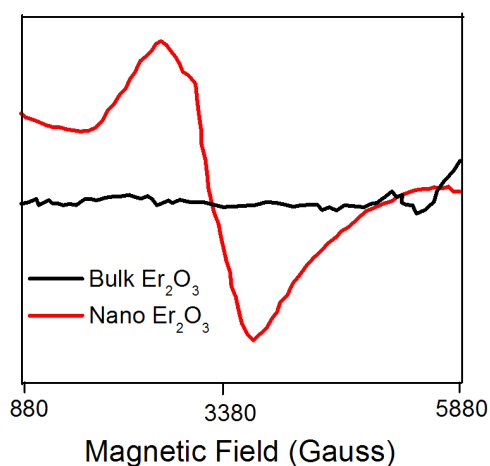


Figure 10 | The EPR spectra for bulk Er_2O_3 and Er_2O_3 NPs at room temperature.

Ho^{3+}), the UC broadband located at 600 nm (~ 2.0 eV) was also observed, which is exactly the same as this work²⁶. The origin of the UC broadband was attributed to the defect emissions related to oxygen defects. Fig. 10 shows the EPR spectra of bulk Er_2O_3 and Er_2O_3 NPs at the room temperature. The microwave frequencies and power are 9.438 GHz and 1 mW, respectively. It can be seen that in bulk Er_2O_3 , the EPR signal was not observed, while in Er_2O_3 NPs, a EPR signal was detected in the range of 880–5580 Gauss with g factor about 1.9951. In general, when the actual measured g factor is lower than the free electron g factor ($g_{\text{free}} = 2.0023$), the EPR signal represents the electron trap³². In other words, the EPR signal in Er_2O_3 NPs is assigned to the oxygen defects. It's known that the bulk material has perfect lattice and little defects, so the EPR signal is not detected in bulk Er_2O_3 . These results further prove that the UC broadband originates from the oxygen defects emission in Er_2O_3 NPs, and it's completely different from the UC broadband in bulk Er_2O_3 reported previously¹⁵.

Based on the above discussions, it is suggested that for the Er_2O_3 NPs and $\text{Ag-SiO}_2\text{-Er}_2\text{O}_3$ nanocomposites samples, the efficient absorption of NIR photons, improved temperature, and oxygen defects are the key important factors for the generation of high-intensity UC broadband. Fig. 11 shows the schematic of the possible mechanism of UC broadband emission in Er_2O_3 NPs and UCL enhancement in $\text{Ag-SiO}_2\text{-Er}_2\text{O}_3$ nanocomposites. In Er_2O_3 , Er^{3+} ions on ground states $^4\text{I}_{15/2}$ are mainly excited to $^4\text{I}_{11/2}$ and $^4\text{I}_{9/2}$ by the first-step ET from excited Er^{3+} under 980 nm and 780–860 nm excitation, through the subsequent nonradiative relaxation of $^4\text{I}_{11/2}$, $^4\text{I}_{9/2}$, the electrons populate to the $^4\text{I}_{13/2}$, $^4\text{I}_{9/2}$ levels, respectively, and then are excited to $^4\text{F}_{7/2}$ and $^2\text{H}_{9/2}$, or $^4\text{F}_{9/2}$ and $^4\text{F}_{5/2}$ by the second-step ET or excited-state absorption. At the low excitation power, the electrons stepwise populate to the $^2\text{H}_{9/2}$, $^4\text{F}_{5/2}$, $^4\text{F}_{5/2}$, $^2\text{H}_{11/2}$, $^4\text{S}_{3/2}$, and $^4\text{F}_{9/2}$, subsequently generating the blue, green and red emissions^{33–35}. As the excitation power is high enough, the temperature of Er_2O_3 or $\text{Ag-SiO}_2\text{-Er}_2\text{O}_3$ samples increases considerably, leading to the cross relaxation ($^4\text{F}_{7/2} + ^4\text{I}_{11/2} \rightarrow ^4\text{F}_{9/2} + ^4\text{F}_{5/2}$) exacerbating. Because the multi-photon ($n > 3$) UCL was not observed in Er_2O_3 or $\text{Ag-SiO}_2\text{-Er}_2\text{O}_3$ samples, it's confirmed that most of the electrons on $^4\text{F}_{9/2}$ are captured by the oxygen vacancy states through the tunneling effect. Meanwhile, on the valence band of Er_2O_3 or $\text{Ag-SiO}_2\text{-Er}_2\text{O}_3$ samples, a large number of holes were generated, which could be confirmed by the occurrence of photocurrent (see Fig. 9). It is suggested that the electrons on oxygen vacancy states recombined with holes in the valence band of Er_2O_3 , generating broadband UCL. (The location of the oxygen vacancy states was confirmed by the UC broadband emission.) It should be pointed out that the radiative transition rate

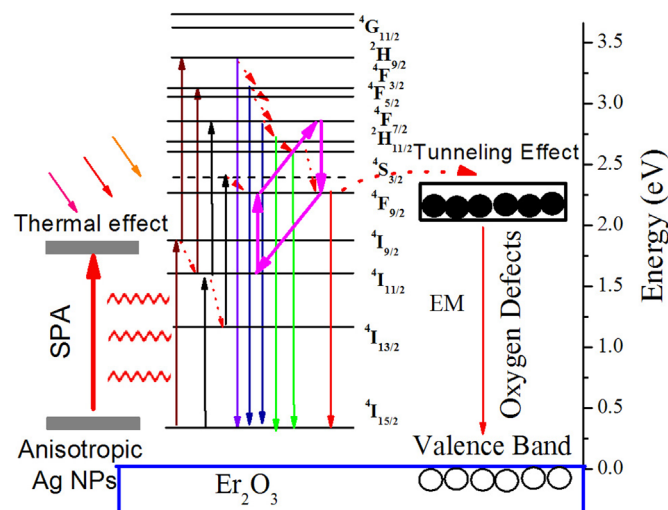


Figure 11 | The schematic of the possible mechanism of UC broadband emission in Er_2O_3 NPs and UCL enhancement in $\text{Ag-SiO}_2\text{-Er}_2\text{O}_3$ nanocomposites.

of electron-hole recombination of semiconductor was at least several orders larger than the $4f\text{-}4f$ transitions of Er^{3+} ions^{36,37}, and thus could exceed the nonradiative relaxation rate of Er^{3+} ions, preventing the thermal quenching of UCL. On the contrary, due to the direct $4f\text{-}4f$ radiative transition rate of excited Er^{3+} ions was much smaller than the nonradiative relaxation rate at elevated temperature, this kind of UCL was unavoidably quenched. And in $\text{Ag-SiO}_2\text{-Er}_2\text{O}_3$ nanocomposites, the improvement of UCL are mainly attributed to the thermal effect with the SP excitation of Ag NPs, which is beneficial to generating thermal holes in the valence band, resulting in the decrease of threshold power for generating white light.

Conclusions

In this paper, $\text{Ag-SiO}_2\text{-Er}_2\text{O}_3$ nanocomposites were prepared by a wet-chemical method and characterized by XRD patterns, TEM images, EDX mapping, and UV-vis absorption spectra. The results show that the anisotropic small Ag NPs distribute randomly and have strong SPA in the range of 400–1000 nm in the composites. In the composites the UCL intensity was improved greatly over that of Er_2O_3 , depending strongly on excitation power of 980-nm laser diode. The enhancement factor changed from several times until to $\sim 10^4$, and under the excitation of 1.5 W/mm², the UCL intensity of $\text{Ag-SiO}_2\text{-Er}_2\text{O}_3$ improved 40 times over the well known $\text{NaYF}_4\text{:Yb}^{3+}, \text{Er}^{3+}$ commercial powders. And more, it should be noted that the UCL of the broadband in $\text{Ag-SiO}_2\text{-Er}_2\text{O}_3$ as well as Er_2O_3 demonstrated favorable two excitation bands, could effectively avoid concentration quenching and temperature quenching. The mechanism of the broadband UCL in Er_2O_3 and $\text{Ag-SiO}_2\text{-Er}_2\text{O}_3$ was attributed to the electron-hole combination and the UCL enhancement in $\text{Ag-SiO}_2\text{-Er}_2\text{O}_3$ was mainly attributed to thermal effect, which dramatically increased the density of holes on the valence band. Overall, the $\text{Ag-SiO}_2\text{-Er}_2\text{O}_3$ composite is a novel favorable UCP with super intense UCL and is promised to work at extreme conditions such as at high pumping power and at high temperature.

Methods

Sample preparation. The specific preparing procedure was as follows, shown in Fig. 1(a). Firstly, the 60-nm silver was prepared through ethylene glycol reduction method⁸. In a typical synthesis process, 3.3 g PVP-K40 was first dissolved in EG at the room temperature, after that 0.14 g AgNO_3 was added and stirred for ten minutes. The mixture was heated to 120°C for an hour, then allowed to cool naturally. The whole process had the protection of nitrogen. The Ag nanoparticles (NPs) were isolated by centrifugation and washed several times with acetone and deionized water. Then, Ag-SiO_2 composites were prepared by the modified STÖBER method²³. The



as-prepared Ag NPs and a small amount of ammonia and TEOS were dissolved in ethanol and stirred for 24 hours at room temperature. Then, the precipitates were collected and washed three times with alcohol. After that, the precipitates (Ag-SiO₂) were dissolved in deionized water, added into Er(NO₃)₃·H₂O and urea, heated at 90 °C for an hour and cleaned with alcohol three times. Then, the obtained sample was annealed at 500 °C for 3 hours²⁴. At last, the Ag-SiO₂-Er₂O₃ composites were collected. For comparison, Er₂O₃ NPs were synthesized by a similar method.

Characterization. The morphology of the products was recorded on a Hitachi H-8100IV transmission electron microscope (TEM) under an acceleration voltage of 200 kV. The energy-dispersive X-ray (EDX) elemental mapping images were recorded on a FEI Tecnai G2 S-Twin microscope under a working voltage of 200 kV equipped with EDX spectrometer. The phase structure and purity of the as-prepared samples were characterized by X-ray power diffraction (XRD) with a Rigaku D/max 2550 X-ray diffractometer, using a monochromatized Cu target radiation resource ($\lambda = 1.54\text{\AA}$). UV/Vis-NIR absorption spectra were measured with a Shimadzu UV-1800PC UV/Vis-NIR scanning spectrophotometer in the range from 300 to 1100 nm. In the measurements of power-dependent UCL spectra, a continuous 980 nm was used to pump the samples. A visible photomultiplier (350–850 nm) combined with a double-grating monochromator were used for spectral collection. In order to obtain the excitation spectra of UCL, the integrated intensity over the 350–720 nm range of the emission was plotted versus excitation wavelength, and that process was fulfilled by using a Titanium: Sapphire oscillator (Mira-HP; Coherent, Santa Clara, CA) which worked in the CW mode which was pumped by a continuous wave laser (Verdi-V18; Coherent). The photo current-voltage (I–V) curves were acquired by a source-measurement unit under the illumination of continuous 980 nm diode laser or Titanium: Sapphire oscillator which worked in the CW mode (790 ~ 830 nm). Electron paramagnetic resonance (EPR) spectra were measured by the JESFE3AX electron spin resonance spectrophotometer at room temperature.

- Auzel, F. Upconversion and Anti-Stokes Processes with f and d Ions in Solids. *Chem. Rev.* **104**, 139 (2004).
- Esterowitz, L., Noonan, J. & Bahler, J. Enhancement in a Ho³⁺-Yb³⁺ quantum counter by energy transfer. *Appl. Phys. Lett.* **10**, 126–127 (1967).
- Rapaport, A., Milliez, J., Bass, M., Fellow, L. & Cassanho, A. Review of the Properties of Up-Conversion Phosphors for New Emissive Displays. *J. Disp. Technol.* **2**, 68–78 (2006).
- Yu, X. F. *et al.* Dopant-Controlled Synthesis of Water-Soluble Hexagonal NaYF₄ Nanorods with Efficient Upconversion Fluorescence for Multicolor Bioimaging. *Nano Res.* **3**, 51–60 (2010).
- Wang, L. Y. *et al.* Fluorescence Resonant Energy Transfer Biosensor Based on Upconversion-Luminescent Nanoparticles. *Angew. Chem. Int. Edit.* **44**, 6054–6057 (2005).
- Wang, F. & Liu, X. G. Recent Advances in the Chemistry of Lanthanide-Doped Upconversion Nanocrystals. *Chem. Soc. Rev.* **38**, 976–98999 (2009).
- Boyer, J. C. & van Veggel, Frank, C. J. M. Absolute Quantum Yield Measurements of Colloidal NaYF₄: Er³⁺, Yb³⁺ Upconverting Nanoparticles. *Nanoscale* **2**, 1417 (2010).
- Xu, W. *et al.* Ultra-broad Plasma Resonance Enhanced Multicolor Emissions in an Assembled Ag/NaYF₄:Yb,Er Nano-film. *Nanoscale* **4**, 6971–6973 (2012).
- Li, A. H. & Lü, Q. Power-dependent Upconversion Luminescence Intensity in NaYF₄: Yb³⁺, Er³⁺ Nanoparticles. *EPL*. **96**, 18001 (2011).
- Mai, H. X., Zhang, Y. W., Sun, L. D. & Yan, C. H. Highly Efficient Multicolor Up-conversion Emissions and Their Mechanisms of Monodisperse NaYF₄:Yb,Er Core and Core/Shell-Structured Nanocrystals. *J. Phys. Chem. C.* **111**, 13721–13729 (2007).
- Bryan, M., Linda, A. & Andries, M. Lanthanide Ions As Spectral Converters for Solar Cells. *Phys. Chem. Chem. Phys.* **11**, 11081–11095 (2009).
- Wang, J. W. & Peter, A. T. Upconversion for White Light Generation by a Single Compound. *J. Am. Chem. Soc.* **132**, 947–949 (2010).
- Strek, W. *et al.* White Emission of Lithium Ytterbium Tetraphosphate Nanocrystals. *Opt. Express*. **19**, 14083–14092 (2011).
- Wang, J. W., Hao, J. H. & Peter, A. T. Luminous and Tunable White-light Upconversion for YAG (Yb₃Al₅O₁₂) and (Yb,Y)₂O₃ Nanopowders. *Opt Lett.* **35**, 3922–3924 (2010).
- Xu, S. *et al.* Observation of Ultrabroad Infrared Emission Bands in Er₂O₃, Pr₂O₃, Nd₂O₃, and Sm₂O₃ Polycrystals. *App. Phys. Exp.* **5**, 102701 (2012).
- Yang, T. S. *et al.* Cubic sub-20 nm NaLuF₄-based Upconversion Nanophosphors for High-contrast Bioimaging in Different Animal Species. *Biomaterials* **33**, 3733–3742 (2012).
- Yi, G. S. & Chow, G. M. Water-Soluble NaYF₄:Yb,Er(Tm)/NaYF₄/Polymer Core/Shell/Shell Nanoparticles with Significant Enhancement of Upconversion Fluorescence. *Chem. Mater.* **19**, 341 (2007).
- Wang, F. *et al.* Tuning Upconversion Through Energy Migration in Core-Shell Nanoparticles. *Nat. Mater.* **10**, 968–973 (2011).
- Schietinger, S., Aichele, T., Wang, H. Q., Nann, Thomas. & Benson, O. Plasmon-Enhanced Upconversion in Single NaYF₄:Yb³⁺/Er³⁺ Codoped Nanocrystals. *Nano. Lett.* **10**, 134–138 (2010).
- Liu, N., Qin, W. P., Qin, G. S., Jiang, T. & Zhao, D. Highly Plasmon-Enhanced Upconversion Emissions from Au@β-NaYF₄:Yb,Tm Hybrid Nanostructures. *Chem. Comm.* **47**, 7671–7673 (2011).
- Zhang, W. H., Ding, F. & Chou, S. Y. Large Enhancement of Upconversion Luminescence of NaYF₄:Yb³⁺/Er³⁺ Nanocrystal by 3D Plasmonic Nano-Antennas. *Adv. Mater.* **24**, OP236–OP241 (2012).
- Saboktakin, M. *et al.* Metal-Enhanced Upconversion Luminescence Tunable through Metal Nanoparticle–Nanophosphor Separation. *ACS Nano.* **6**, 8758–8766 (2012).
- Zhang, R. H. *et al.* Surface-Enhanced Fluorescence from Fluorophore-Assembled Monolayers by Using Ag@SiO₂ Nanoparticles. *ChemPhysChem.* **12**, 992–998 (2011).
- Rai, V. K. *et al.* Surface-plasmon-enhanced Frequency Upconversion in Pr³⁺-Doped Tellurium-oxide Glasses Containing Silver Nanoparticles. *J. Appl. Phys.* **103**, 093526 (2008).
- Link, S., Mohamed, M. B. & El-Sayed, M. A. Simulation of the Optical Absorption Spectra of Gold Nanorods as a Function of Their Aspect Ratio and the Effect of the Medium Dielectric Constant. *J. Phys. Chem. B.* **103**, 3073–3077 (1999).
- Zhu, Y. S. *et al.* Broad White Light and Infrared Emission Bands in YVO₄:Yb³⁺,Ln³⁺ (Ln³⁺ = Er³⁺, Tm³⁺, or Ho³⁺). *Appl. Phys. Exp.* **5**, 092701–3 (2012).
- Polosan, S., Bettinelli, M. & Tsuboi, T. Photoluminescence of Ho³⁺:YVO₄ Crystals. *Phys. Status Solidi (C)*. **4**, 1352–1355 (2007).
- Saad, A. M., Mohamed, M. B., Abou Kana, M. T. H. & Azzouz, I. M. Synthesis Effect, Upconversion and Amplified Stimulated Emission of Luminescent CdTe NPs. *Optics & Laser Technology.* **46**, 1–5 (2013).
- Liu, Y. B. *et al.* Single-nanocrystal Sensitivity Achieved by Enhanced Upconversion Luminescence. *Nature Nanotech.* **8**, 729–734 (2013).
- Redmond, S., Rand, S. C., Ruan, X. L. & Kaviany, M. Multiple Scattering and Nonlinear Thermal Emission of Yb³⁺, Er³⁺:Y₂O₃ Nanopowders. *J. Appl. Phys.* **95**, 4069 (2004).
- Subba Rao, G. V., Ramdas, S., Mehrotra, P. N. & Rao, C. N. R. Electrical Transport in Rare-earth Oxides. *J. Solid. State Chem.* **2**, 377–384 (1970).
- Liu, Y., Wan, S. L. & Li, X. G. Visualizing High-temperature Spin Dynamics in La_{1-x}Ca_xMnO₃ from a Mapping of EPR Linewidth and g-factor. *J. Phys.:Condens. Matter.* **19**, 196213 (2007).
- Wang, J. *et al.* Enhancing Multiphoton Upconversion Through Energy Clustering at Sublattice Level. *Nature Mater.* **13**, 157–162 (2014).
- Liu, Y. S., Tu, D. T., Zhu, H. M. & Chen, X. Y. Lanthanide-doped Luminescent Nanoprobes: Controlled Synthesis, Optical Spectroscopy, and Bioapplications. *Chem. Soc. Rev.* **42**, 6924–6958 (2013).
- Huang, P. *et al.* Lanthanide-Doped LiLuF₄ Upconversion Nanoprobes for the Detection of Disease Biomarkers. *Angew. Chem. Int. Ed.* **53**, 1252–1257 (2014).
- Koch, S. W., Kira, M., Khitrova, G. & Gibbs, H. M. Semiconductor Excitons in New Light. *Nat. Mater.* **5**, 523–531 (2006).
- Xiao, K. & Yang, Z. Blue Cooperative Luminescence In Yb³⁺-Doped Barium Gallogermanate Glass Excited At 976 nm. *J. Fluoresc.* **16**, 755–759 (2006).

Acknowledgments

This work was supported by the Major State Basic Research Development Program of China (973 Program) (No. 2014CB643506), the National Natural Science Foundation of China (Grant No. 11374127, 11304118, 61204015, 81201738, 61177042, and 11174111), Program for Chang Jiang Scholars and Innovative Research Team in University (No. IRT13018).

Author contributions

W.X. conducted the most of investigation for the samples and wrote the main paper. H.W.S. supervised the project, had given valuable advices on the proceeding of this work, and revised the manuscript. X.L.M., X.C. and Y.S.Z. had provided precious suggestions on the selection of up-conversion broad band phosphors. S.B.C. and L.T. supported the characterization of the samples. P.W.Z. and S.X. had provided precious suggestions on the photocurrent and EPR test. All authors discussed the results and commented on the manuscript at all stages.

Additional information

Supporting Information Available: The UCL spectra of Ag-SiO₂-Er₂O₃ composites under 808 nm excitation; UCL enhancement in Ag-SiO₂-Y₂O₃:Yb,Er nanocomposites; The power density dependence of photocurrent of Er₂O₃ NPs, Ag-SiO₂-Er₂O₃ composites on excitation power of 980 nm light.

Supplementary information accompanies this paper at <http://www.nature.com/scientificreports>

Competing financial interests: The authors declare no competing financial interests.

How to cite this article: Xu, W. *et al.* Ag-SiO₂-Er₂O₃ Nanocomposites: Highly Effective Upconversion Luminescence at High Power Excitation and High Temperature. *Sci. Rep.* **4**, 5087; DOI:10.1038/srep05087 (2014).



This work is licensed under a Creative Commons Attribution-NonCommercial-NoDerivs 3.0 Unported License. The images in this article are included in the article's Creative Commons license, unless indicated otherwise in the image credit;

if the image is not included under the Creative Commons license, users will need to obtain permission from the license holder in order to reproduce the image. To view a copy of this license, visit <http://creativecommons.org/licenses/by-nc-nd/3.0/>